

1D Photonic Crystal-Based Biosensor for Multiple Biomarkers Detection

Farzaneh Bayata^{*}, Kazem Jamshidi-Ghaleha

^aDepartment of Physics, Azarbaijan Shahid Madani University, Tabriz, East Azarbaijan, Iran

^{*}Corresponding author email: f.bayat@azaruniv.ac.ir

Received: Dec. 6, 2022, Revised: Jan. 5, 2023, Accepted: Feb. 15, 2023, Available Online: Feb. 25, 2023

DOI: 10.30495/ijbbe.2023.1974383.1019

ABSTRACT— In this paper, a highly sensitive 1D photonic crystal (1DPC) based biosensor is introduced and theoretically studied using the transfer matrix method, which has the capability of detecting multiple biomarkers, simultaneously. An m by n gradient refractive index (GRIN) lens array is introduced to the center of a 1DPC structure as a defect layer that is surrounded by two microfluidic channels. By irradiating a natural light source to the structure, a multiple array of the concentric rainbow appears on the output plane. The frequency range of these rainbows is highly dependent on the effective refractive index of the fluid inside the two microfluidic channels. By functionalizing the surfaces around the channels with an m by n antibody array along with the interaction of the various biomarkers, each element of the rainbow array displays the changes in the concentration of a different biomarker. Any change in the concentration of the biomarkers can cause a variation in the effective refractive index of the fluid and thus lead to a shift in the generated rainbow frequency range of the output. The size and number of the generated rainbow array may be engineered by using the central defect layer's refractive index distribution function.

KEYWORDS: Biosensors, Defect layers, Gradient refractive index lenses, One-dimensional photonic crystals, Transfer matrix method.

I. INTRODUCTION

Detecting multiple biomarkers in a single set-up on lab-on-a-chip devices attracts a lot of attention these days. Being able to detect hundreds of biomarkers at the same time can help us to save the time and cost of the experiments. Thus, different efforts are focused on designing such sensors. Recently, surface plasmon resonance imaging (SPRI) has been of great interest to researchers. SPRI is the variation of SPR that makes the multiple adsorption interaction possible. In SPRI, the SPR chip is functionalized with an antibody array. So, a different part of the chip is ready to adsorb a special biomarker. Therefore, the refractive index changes of the environment above the gold layer are due to the presence of these biomarkers. As an example, in ref [1], 264 different ligands are immobilized on the chip

and their interrogating binding events are investigated. Also, Fu and Yager et al. reported an SPR imaging system operating with 400 pixels [2]. In SPRI, both sensorgrams and chip images are recorded using a CCD camera [3], [4]. The creation of antibody microarrays can be done using different methods such as dip-pen nanolithography [5]–[7], micro-contact printing [8], [9], atomic force microscopy (AFM)-based nanografting [10], and SNOM (scanning near-field optical microscopy) lithography [11]. Using the mentioned methods, it is possible to make antibody microarrays output print of 48 different antibody spots with a diameter of 10 μm , simultaneously [12]. On the other hand, artificial PC structures have been studied widely due to their ability to control light and widespread applications [13]. For the structures of certain symmetries with sufficiently high dielectric contrast, there is a certain range of

frequencies that the photon density of states is completely blocked. This full photonic bandgap (PBG) has important effects on photonics technology because of the possibility of reducing spontaneous emission in certain semiconductor devices [14]. It is possible to generate highly localized defect modes in the PBG by breaking the periodicity and adding a defect layer into the structure [15]. In our previous papers[16]–[19], we introduced different type of laser beam that were generated using the PBG properties of 1DPC nanostructures. We broke the periodicity of the PC structure by adding a graded-index defect layer. According to the refractive index distribution function, different incident rays experience different ray paths, with modulated defect mode, output phase, and generated intensity. Also, using the advantages of the generated laser beam, we have been able to add two microfluidic channels in order to implement both a biosensor and a chemical one that could detect the refractive index variation of fluid flowing in the channels with smallest value of Δn being 1×10^{-4} RIU in real-time [19]. In this paper, we have studied theoretically a 1D photonic crystal-based biosensor that could detect multiple biomarkers simultaneously. The basic sensing method is similar to our previous method [19] that is, we have provided a way to improve the capability of previous sensor for multiple biomarkers detection. This has been accomplished by adding a new defect layer having a spatial refractive index distribution function. Thus, Using the introduced biosensor, it is possible to investigate the concentration of the different biomarkers in a fluid at the same time. Therefore, the proposed biosensor may be considered as a cost effective and less time consuming method that may be used for that facilitation of medical experiments.

II. MODELING AND THEORY

We study the arrangement of $(AB)^7 F D F (AB)^7$ that is a binary defective 1DPC structure, using the transfer matrix method, where A and B are consist of $ZnSe$ and SiO_2 with the refractive indexes of 2.6 [20] and 1.05 [21] respectively. This structure may be implemented in practice by the oblique-angle deposition method [22].

Also, F represents the microfluidic channel and D stands for an m by n GRIN lens array. Such a GRIN lens array is also may be fabricated using photopolymerization method [23], [24]. Considering numerical calculations, the D

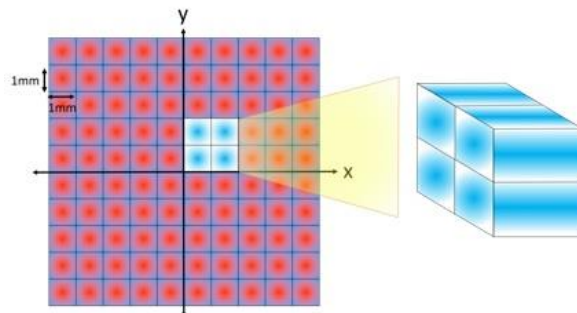


Fig. 1 Refractive index distribution of the gradient defect layer (D) with 10×10 array of GRIN lenses. In numerical calculations, blue elements of the lens array are considered.

layer's refractive index distribution function is

$$\text{defined by } n = n_0 \left(1 + a \sin^2 \left(\frac{x}{b} \right) \sin^2 \left(\frac{y}{d} \right) \right) \text{ in}$$

Coordinates $(x - y)$, where $n_0 = 1.608$ is the background refractive index and a is a constant that can specify by the rate of the refractive index variation in each of the array elements [19]. with the b and d being the array's dimension. In our study, we have chosen $b = d = 1 \text{ mm}$ and $a = (0.608)^2$. So, if the lateral dimension of the structure and accordingly the D layer is taken to be $1 \text{ cm} \times 1 \text{ cm}$, we then will have a defect layer with a 10×10 the array of GRIN lenses that are shown in Fig. 1. For simplicity, the numerical calculations are done for the structure with the lateral dimension of $2 \text{ mm} \times 2 \text{ mm}$ with the so called, four-elemental GRIN lens array that is shown in Fig. 1. The same results can be obtained for a wider 1DPC structure which contains a defect layer with more elements of the GRIN lens array. The schematic of the designed biosensor structure is shown in Fig. 2. To simulate a structure that is also practical, it is suggested to design a structure that is separable into three parts. The central GRIN layer is surrounded by a frame. The frame should be designed in a way that by attaching PC slabs to it, two empty spaces will remain around it that can be supposed as microfluidic channels. So, the layers around the channels can be functionalized by an antibody

array before attaching the whole structure. The dimension of this antibody array needs to be similar to the dimension of the GRIN lens array. The whole structure is irradiated by a white light source and the output light is detected on the output plane. Having designed the structure, let us consider a propagating plane wave in the z-direction that is incident normally into the proposed structure. The well-known transfer matrix method [25], which is one of the simplest and most common methods to analyze the optical spectrum of 1DPC structures, is employed in the calculations. According to this

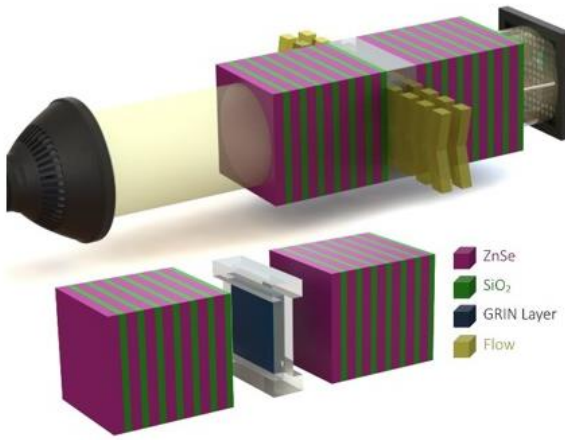


Fig. 2 The schematic of the designed biosensor with the irradiated natural light source and the detector output.

method, during the propagation of an electromagnetic wave in the PC structure, the electric vector E and the magnetic vector H , between one layer and its neighbor are related with the following matrix:

$$M_j(\omega) = \begin{bmatrix} \cos k_j d_j & \frac{i}{n_j} \sin k_j d_j \\ i n_j \sin k_j d_j & \cos k_j d_j \end{bmatrix} \quad (1)$$

where $i = \sqrt{-1}$, $k_j = \frac{n_j \omega}{c}$, c is the speed of light in the vacuum and d_j is the thickness of layers in which $j = A, B, F$ and D . For the complete structure, the total transfer matrix function is as follows :

$$M(r, \omega) = [M_A(\omega)M_B(\omega)]^7 M_F(r, \omega)M_D(r, \omega)M_F(r, \omega) \\ [M_A(\omega)M_B(\omega)]^7 = \begin{bmatrix} m_{11}(r, \omega) & m_{12}(r, \omega) \\ m_{21}(r, \omega) & m_{22}(r, \omega) \end{bmatrix} \quad (1)$$

To determine the transmission coefficient in the free space, the total characteristic matrix elements are used as:

$$t(r, \omega) = \frac{2}{[m_{22}(r, \omega) + m_{11}(r, \omega)] - [m_{12}(r, \omega) + m_{21}(r, \omega)]} \quad (3)$$

The real and imaginary parts of $t(r, \omega)$ are applied to calculate the amplitude of the transmitted wave. The transmittance is given by $T(r, \omega) = |t(r, \omega)|^2$.

III. NUMERICAL RESULTS AND DISCUSSIONS

Using numerical calculations, the quarter-wave is taken for the thickness of the layers; $n_A d_A = n_B d_B = n_0 d_D = d_F = \lambda_0 / 4$, with λ_0 being the design wavelength ($= 550$ nm) where d_A , d_B , d_D and d_F are the thickness of layers A , B , D , and F , respectively. Figure 3 shows the transmitted light from the structure, versus the

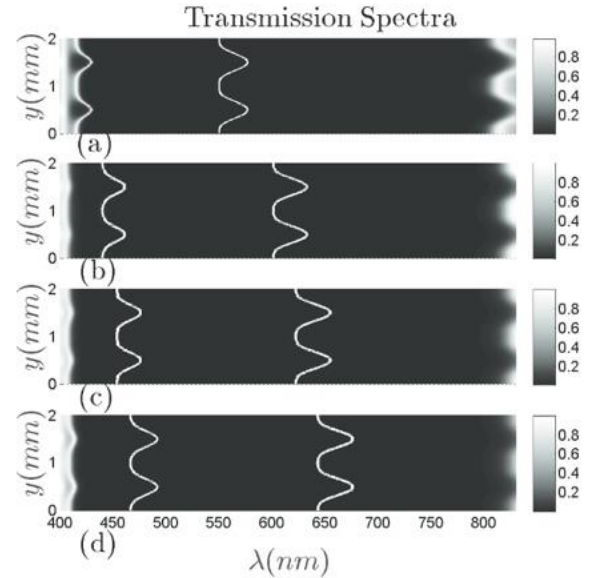


Fig. 3 The schematic of the designed biosensor that is irradiated by natural light source with the detector output.

incident beam wavelength, This also has been accomplished for transverse Cartesian Coordinate (y) for four different fluids with different refractive indexes inside the microfluidic channels. As it can be seen in this figure, the consequence of adding a defect layer with the proposed spatial refractive index distribution function to the periodic structure, is a spatially distributed defect mode in the PBG. The refractive index variation of the fluid can cause a shift in the PBG and defect modes. To have a spatial point of view, the 4D illustration of the defect modes is shown in Fig. 4.

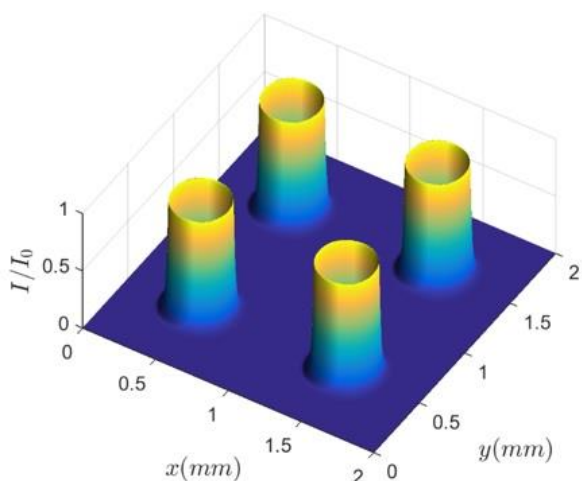


Fig. 4 Profile of the normalized intensity distribution on the output plane versus Cartesian Coordinates ($x-y$) for incident beam wavelength of 635 nm and $n_F = 1.3$.

versus Cartesian Coordinates ($x - y$) and incident beam wavelengths in the range of 620

nm to 660 nm. If a wavelength in the range of defect modes is chosen and a light beam with

this wavelength is irradiated to the structure, an array of ring-shaped intensity distribution with a special diameter will appear on the output plane (Fig. 5).

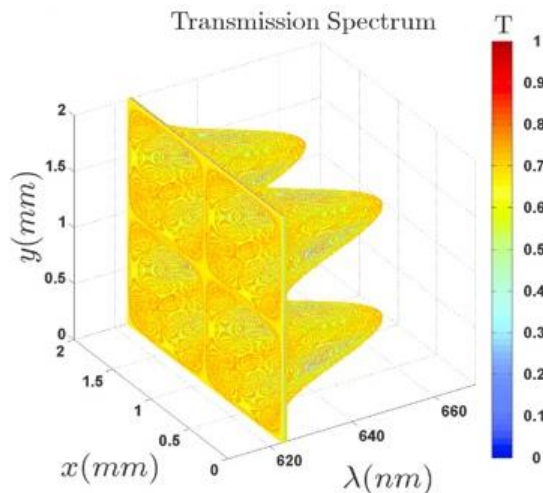


Fig. 5 4D illustration of the spatial defect modes. The transmission spectrum of the 1DPC structure with proposed graded-index defect layer under the irradiation of the plane wave beam versus the incident beam wavelength and Cartesian Coordinates ($x-y$) in the first bandgap for $n_F = 1.35$. (The fourth dimension, which is transmission, is shown in color).

Therefore, by irradiating a white light to the structure, concentric rings of different wavelengths (concentric rainbow) can appear on the output plane. The side view of the concentric rainbow array element of (1, 1) for some wavelengths is shown in Fig. 6.

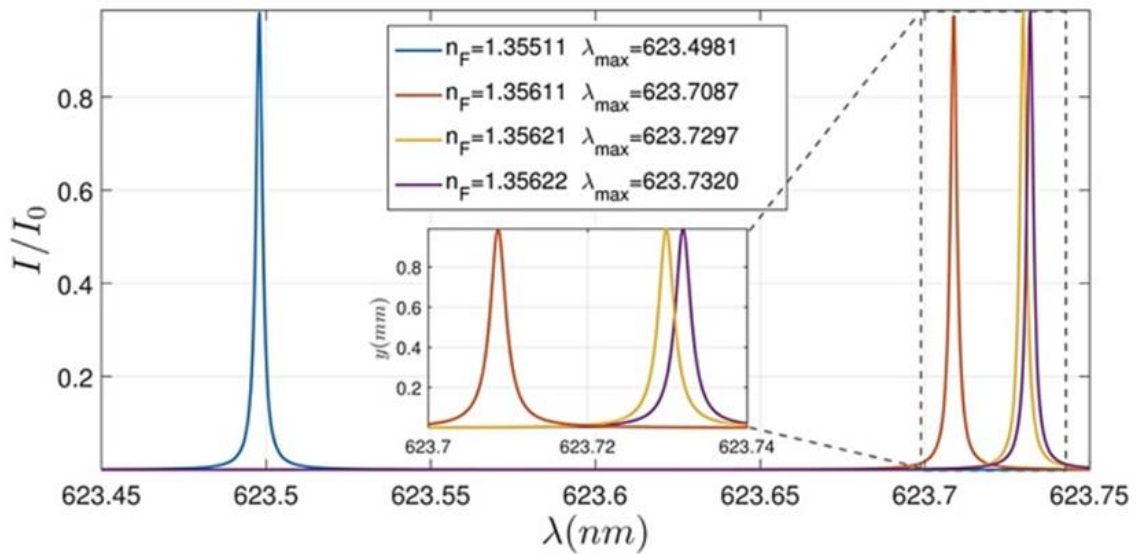


Fig. 6 The detected spectrum for the pixel element at $x = 0.5 \text{ mm}$ and $y = 0.5 \text{ mm}$ for different effective refractive index of the fluid.

By flowing different fluids inside the channels, the concentric intensity rings in a different range of wavelengths will appear on the output plane that can be detected by different methods. In this step, to improve the proposed biosensor to a selective one and also detect multiple biomarkers, functionalization of the surfaces around the microfluidic channels with an m by n antibody array is suggested. The dimension of the antibody array that is immobilized on these surfaces is the same as the dimension of the GRIN lens array. It means that, in our introduced structure, each of the $1 \text{ mm} \times 1 \text{ mm}$ squares on the surfaces around the channels is functionalized with a special antibody (As it is shown in Fig. 1). Therefore, by flowing a fluid

containing different biomarkers inside the channels, each biomarker is going to attach to its antibody and the fluid keeps flowing in the channels. So, the concentration of each biomarker is going to increase in different parts

of the channels that creates an m by n array of biomarkers concentration in the fluid. Then, various spatial parts of the propagating beam inside of the channels face different effective refractive indices of the fluid. It influences the output beam's spectral range in each of the output concentric rainbow arrays. In fact, the effect of the presence of each biomarker attached to the antibody array's element in the m^{th} column and n^{th} row can be seen in the rainbow element in the m^{th} column and n^{th} row. So being able to, to detect multiple biomarkers simultaneously with only a single white light source, we have suggested a novel biosensor that can be comparable with SPRI. To obtain the sensitivity of the introduced biosensors, some limits of detection should be considered. For that two factors may limit the sensitivity of the proposed sensor. The first one is the spectral beam width of the output beam. As it was stated in our previous study [19], it

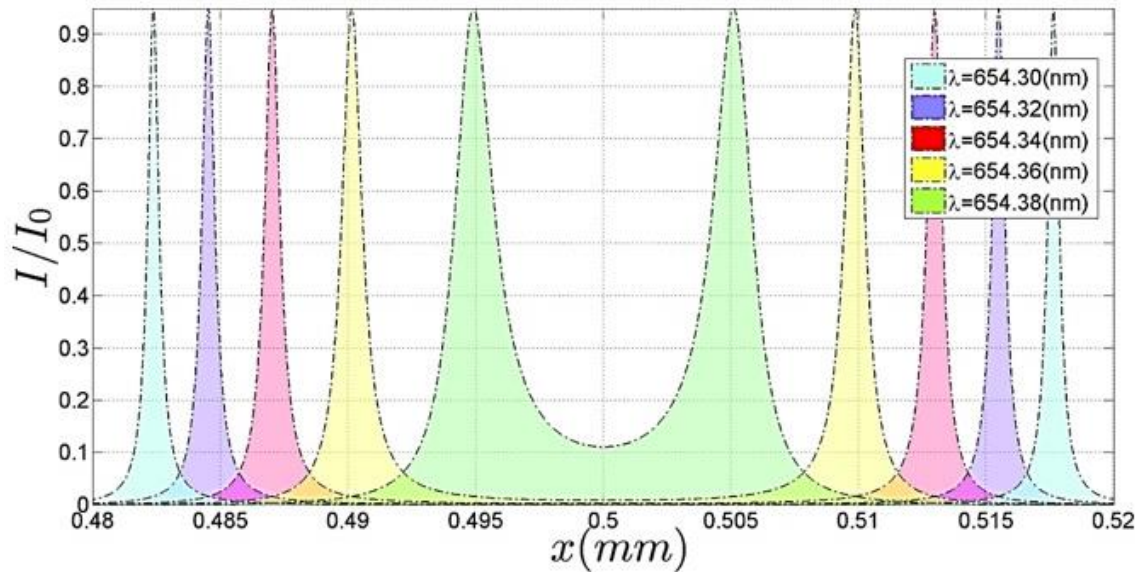


Fig. 7 The side view of the concentric rainbow array element of (1,1) for some selected wavelengths.

highly depends on the number of layers of the structure. By increasing the number of layers, the spectral and spatial beam width is going to decrease. In this study, having considered the cost of the fabrication in practice and the possibility of the intensity distribution detection on the output plane, we have optimized the number of layers to be 7. Figure 7 displays the detected spectrum in a pixel element placed at $x = 0.5 \text{ mm}$ and $y = 0.5 \text{ mm}$ for the rainbow array element of (1, 1) on the output plane. As it is clear in this figure, for the fluid's effective refractive index variation of $\Delta n = 1 \times 10^{-3} \text{ RIU}$, $\Delta n = 1 \times 10^{-4} \text{ RIU}$, and $\Delta n = 1 \times 10^{-5} \text{ RIU}$ the wavelength variation is $\Delta \lambda = 0.2 \text{ nm}$, $\Delta \lambda = 0.02 \text{ nm}$, and $\Delta \lambda = 0.002 \text{ nm}$, respectively. Now, to make the suggested biosensor practical, we need a detecting technique that can detect these wavelength variations. The detecting method plays a significant role in defining the spectral resolution of the introduced biosensor. Two different detecting methods can be suggested for this model: a hyperspectral camera or a spectrometer. Each of these methods has some advantages and disadvantages in this model. A hyperspectral camera, which gives the light intensity of a large number of spectral bands, makes a real-time measurement possible for all the elements of the rainbow array at the same time, although its spectral resolution is very low in comparison with some spectrometers. On the other hand, using a spectrometer, the whole out-

put plane should be scanned by it which takes time and the measurement is not done in the real-time anymore. But, according to the state of the art, high-resolution spectrometers are commercialized that using these types of spectrometers, it is possible to detect spectral displacement of the concentric rainbows with the resolution that meets the highest possible resolution of the designed biosensor ($\Delta n = 1 \times 10^{-5}$). As it was discussed before, the numerical results can be expanded for a wider 1DPC structure that contains a central defect layer with an m by n lens array and a wider light source that is irradiated to the structure. So, we are going to be able to detect multiple biomarkers, using a single set-up, with high sensitivity. Furthermore, it should be considered that the specific binding, any non-specific binding, and the bulk refractive index shift can influence the obtained results. In practice, we need to eliminate the unwanted factors that can affect the measured response. To do that, the experiment can be done twice using a buffer with and without an analyte. Therefore, by comparing the results, the impact of the unwanted factors can be removed.

IV. CONCLUSION

In summary, we have designed and theoretically studied a 1DPC-based biosensor that has the capability of detecting multiple biomarkers using a single setup. The main characteristic of the introduced PC used here is

its central defect layer with two microfluidic channels around it. The central defect layer is an m by n array of GRIN lenses that has a spatial refractive index distribution function. As a result of the presence of this layer, the photonic crystal is going to have a spatial PBG. By irradiating a white light source to the structure, an array of concentric rainbows appears on the output plane that has the same dimension as the array of GRIN lenses in the central defect layer with its frequency range highly depends on the effective refractive index of the fluid flowing in the channels. Using the advantages of this concentric rainbow array, it is possible to detect the presence of multiple biomarkers in the microfluidic channels by functionalizing the layers around the microfluidic channels with an m by n antibody array. Due to the presence of the antibody array, different biomarkers floating in the fluid are going to be attach to their antibodies. Then, the concentration of each biomarker is going to increase in the different parts of the fluid that can make a fluid with an m by n array of concentrations. The number of biomarkers that can be detected using the proposed biosensor can be engineered by the refractive index distribution function of the central defect layer and the width of the light source that is irradiated to the structure. In this paper , numerical calculations are done to show the possibility of detecting 4 biomarkers with the application of a white light source having a diameter of 2 mm. It is easily possible to extend the results for the wider light source and design a biosensor with the ability to detect many biomarkers. Being able to detect multiple biomarkers simultaneously, that may be cost effective and less time consuming procedure for medical applications.

ACKNOWLEDGMENT

The authors would like to thank Azarbaijan Shahid Madani University for its support.

REFERENCES

- [1] E. Ouellet, C. Lausted, T. Lin, C. W. T. Yang, L. Hood, and E. T. Lagally, "Parallel microfluidic surface plasmon resonance imaging arrays," *Lab Chip*, vol. 10, no. 5, pp. 581–588, 2010.
- [2] E. Fu, T. Chinowsky, J. Foley, J. Weinstein, and P. Yager, "Characterization of a wavelength-tunable surface plasmon resonance microscope," *Review of scientific instruments*, vol. 75, no. 7, pp. 2300–2304, 2004.
- [3] B. P. Nelson, T. E. Grimsrud, M. R. Liles, R. M. Goodman, and R. M. Corn, "Surface plasmon resonance imaging measurements of DNA and RNA hybridization adsorption onto DNA microarrays," *Analytical Chemistry*, vol. 73, no. 1, pp. 1–7, 2001.
- [4] S. Scarano, M. Mascini, A. P. F. Turner, and M. Minunni, "Surface plasmon resonance imaging for affinity-based biosensors," *Biosensors and bioelectronics*, vol. 25, no. 5, pp. 957–966, 2010.
- [5] L. M. Demers, D. S. Ginger, S.-J. Park, Z. Li, S.-W. Chung, and C. A. Mirkin, "Direct patterning of modified oligonucleotides on metals and insulators by dip-pen nanolithography," *Science*, vol. 296, no. 5574, pp. 1836–1838, 2002.
- [6] J.-H. Lim, D. S. Ginger, K.-B. Lee, J. Heo, J.-M. Nam, and C. A. Mirkin, "Direct-write dip-pen nanolithography of proteins on modified silicon oxide surfaces," *Angewandte Chemie International Edition*, vol. 42, no. 20, pp. 2309–2312, 2003.
- [7] K. Salaita, Y. Wang, and C. A. Mirkin, "Applications of dip-pen nanolithography," *Nature nanotechnology*, vol. 2, no. 3, pp. 145–155, 2007.
- [8] A. Bernard, J. P. Renault, B. Michel, H. R. Bosshard, E. Delamarche, and Others, "Microcontact printing of proteins," *Advanced Materials*, vol. 12, no. 14, pp. 1067–1070, 2000.
- [9] S. Gupta, K. P. Manubhai, V. Kulkarni, and S. Srivastava, "An overview of innovations and industrial solutions in Protein Microarray Technology," *Proteomics*, vol. 16, no. 8, pp. 1297–1308, 2016.
- [10] M. Castronovo and D. Scaini, "The atomic force microscopy as a lithographic tool: nanografting of DNA nanostructures for biosensing applications," *DNA Nanotechnology: Methods and Protocols*, vol. 749, pp. 209–221, 2011.

- [11] S. R. Coyer, A. J. Garcia, and E. Delamarche, "Facile Preparation of Complex Protein Architectures with Sub-100-nm Resolution on Surfaces," *Angewandte Chemie International Edition*, vol. 46, no. 36, pp. 6837–6840, 2007.
- [12] L. Petersson, L. Dexlin-Mellby, A. A. Bengtsson, G. Sturfelt, C. A. K. Borrebaeck, and C. Wingren, "Multiplexing of miniaturized planar anti-body arrays for serum protein profiling - a biomarker discovery in SLE nephritis," *Lab Chip*, vol. 14, no. 11, pp. 1931–1942, 2014.
- [13] J. W. Strutt, "On waves propagated along the plane surface of an elastic solid," *Proc. London Math. Soc.*, vol. 17, no. 253, pp. 4–11, 1885.
- [14] R. K. Lee, Y. Xu, and A. Yariv, "Modified spontaneous emission from a two-dimensional photonic bandgap crystal slab," *JOSA B*, vol. 17, no. 8, pp. 1438–1442, 2000.
- [15] V. V. Romyantsev and A. Schwartzman, "Peculiarities of propagation of electromagnetic excitations through nonideal 1d Photonic Crystal," *J Electr Electron Syst*, vol. 1, no. 109, pp. 2-7, 2013.
- [16] K. Jamshidi-Ghaleh, F. Bayat, A. Phirouznia, and S. Soleimani, "Petal-shaped optical vortice generation by a graded-index defective 1DPC nanostructure under irradiation of a Gaussian beam," *Journal of Optics*, vol. 17, no. 3, pp. 35104, 2015.
- [17] K. Jamshidi-Ghaleh and F. Bayat, "Engineering 1DPC defect mode with GRIN lenses to design beam shapers," *IEEE Photonics Technology Letters*, vol. 26, pp. 440–443, Mar 2014.
- [18] K. Jamshidi Ghaleh and F. Bayat, "Generating frequency dependant twisted beam shapes using 1DPC nanostructure with graded-index defect layer," *Optics Letters*, vol. 39, no. 13, pp. 3802–3805, 2014.
- [19] F. Bayat, S. Ahmadi-Kandjani, and H. Tajalli, "Designing real-time biosensors and chemical sensors based on defective 1-D Photonic Crystals," *IEEE Photonics Technology Letters*, vol. 28, pp. 1843–1846, Sep 2016.
- [20] Qi, H., X. Zhang, M. Jiang, Q. Wang, and D. Li. "Optical constants of zinc selenide in visible and infrared spectral ranges." *Journal of Applied Spectroscopy* 84, no. 4, pp. 679-682, 2017.
- [21] J.-Q. Xi, Martin F. Schubert, Jong Kyu Kim, E. Fred Schubert, Minfeng Chen, Shawn-Yu Lin, W. Liu & J. A. Smart, "Optical thin-film materials with low refractive index for broadband elimination of Fresnel reflection," *Nature photonics*, vol.1, no. 3, pp. 176-179, 2007.
- [22] J.-Q. Xi, M. F. Schubert, J. K. Kim, E. F. Schubert, M. Chen, S.-Y. Lin, W. Liu, and J. A. Smart, "Optical thin-film materials with low refractive index for broadband elimination of Fresnel reflection," *Nature photonics*, vol. 1, no. 3, pp. 176–179, 2007.
- [23] C. Ye and R. R. McLeod, "GRIN lens and lens array fabrication with diffusion-driven photopolymer," *Optics Letters*, vol. 33, no. 22, pp. 2575–2577, 2008.
- [24] H.-B. Sun and S. Kawata, "Two-photon photopolymerization and 3D lithographic microfabrication," in *NMR 3D Analysis Photopolymerization*, pp. 169–273, Springer, 2004.
- [25] A. Yariv and P. Yeh, "Optical Waves in Crystals: Propagation and Control of Laser Radiation", vol. 5. Wiley New York, pp. 155-219, 1984.